Influence of Monomer Structures for Polymeric Multivalent Ligands: Consideration of the Molecular Mobility of Glycopolymers

Nagao, Masanori
Department of Chemical Engineering, Kyushu University

Kichize, Masaya
Department of Chemical Engineering, Kyushu University

Hoshino, Yu
Department of Chemical Engineering, Kyushu University

Miura, Yoshiko
Department of Chemical Engineering, Kyushu University

出版情報：Biomacromolecules. 22 (7), pp.3119-3127, 2021-07-12. American Chemical Society
バージョン：
権利関係：

Influence of Monomer Structures for Polymeric Multivalent Ligands: Consideration of the Molecular Mobility of Glycopolymers

Masanori Nagao*, Masaya Kichize, Yu Hoshino, and Yoshiko Miura*

Department of Chemical Engineering, Kyushu University, 744 Motooka Nishi-ku, Fukuoka 819-0395, Japan
Email: miuray@chem-eng.kyushu-u.ac.jp

ABSTRACT

Molecular mobility is important for interactions of biofunctional polymers with target molecules. Monomer structures for synthetic biofunctional polymers are usually selected based on their compatibility with polymerization systems, whereas the influence of monomer structures on the interaction with target molecules is hardly considered. In this report, we evaluate the correlation between the monomer structures of glycopolymers and their interactions with concanavalin A (ConA) with respect to the molecular mobility. Two types of glycopolymers bearing mannose are synthesized with acrylamide or acrylate monomers. Despite the similar structures, except for amide or ester bonds in the side chains, the acrylate-type glycopolymers exhibit stronger interaction with ConA both in the isothermal titration calorimetry measurement and in a hemagglutination inhibition assay. Characterization of the acrylate-type glycopolymers suggests that the higher binding constant arises from the higher molecular mobility of mannose units, which results from the rotational freedom of

ester bonds in their side chains.

KEYWORDS: Reversible addition-fragmentation chain transfer (RAFT) polymerization, glycopolymers, differential scanning calorimetry (DSC), isothermal calorimetry (ITC), T_2 relaxation, molecular mobility

Introduction

Molecular dynamics based on the flexibility of the polymer structures are important factors for biomacromolecules. Proteins are types of biomacromolecules and have rigid backbone structures that are composed of amino acids. The rigidity of the amide bonds affords their well-defined structures, which display the functional groups of amino acids in three-dimensional space.[1,2] While the precise spatial arrangement of the functional groups enables the intermolecular interactions of proteins, the molecular dynamics are also crucial for further functions. For example, some catalyst activities of enzymes arise from the fluctuation of the polymer structures.[3–7] The flexible polymer structure of an enzyme enables the smooth binding and release of target molecules during the catalyzed reaction. The balance between the rigidity and flexibility of polymer structures is a critical parameter for biomolecular recognition.

Multivalent interaction is a ubiquitous mechanism in molecular recognition of biomacromolecules.[8] Interactions between biomolecules are enhanced by the accumulation of weak interactions. For example, antibodies bind to antigens through the accumulation of interactions among the functional groups of amino acids such as hydrogen bonds, electrostatic interactions, and hydrophobic interactions. This mechanism has been used as a design criterion of efficient ligands for biomolecules, and synthetic ligands that have multiple functional units to interact with target molecules have been reported. [9–13]

The interactions between multivalent ligands and target molecules are interpreted by Gibbs free

energy (ΔG). The value of ΔG was presented by the sum of the enthalpy term (ΔH) and the entropy term ($-T\Delta S$), and the lower ΔG indicates the advantageous for the complex formation ($\Delta G = \Delta H - T\Delta S$).[14] In terms of thermodynamics, the flexibility (or rigidity) of the polymer structures is expected to provide both of favorable and unfavorable influence for the interaction with target molecules.[15,16] The flexibility would enhance the probability of contact between the functional units and the binding sites of the target molecules, which is favorable for the complex formation. Conversely, the flexible polymer ligands would lose the entropy (ΔS) in the complex formation, which is unfavorable. Such a "trade-off" relationship is often observed in the biomolecular interactions and is called as "enthalpy-entropy compensation".[14] This phenomenon indicates that the flexibility of the ligand structure is an important factor in designing the multivalent ligands.

Synthetic biofunctional polymers can be prepared by polymerization of functional monomers and can exhibit a multivalent interaction with biomolecules. To synthesize useful biofunctional polymers that strongly interact with target biomolecules, precise control of the spatial arrangement of functional units toward the structures of target molecules is required when referring to natural proteins.[17–19] To achieve the precise control of biofunctional polymer structures, controlled polymerization techniques are required, where living radical polymerization is a particularly promising technique.[20–24] "Living" radical polymerization allows the use of aqueous solvent, which is an ideal solvent for most biomolecules, and structural parameters such as monomer sequence and molecular weights, are effectively controlled owing to the livingness of the polymer chains.[25–29]

Synthetic biofunctional polymers that recognize target molecules have been synthesized with a few types of acrylic monomers by living radical polymerization. Acrylamide, acrylate, and methacrylate monomers are mainly used to prepare the functional polymers, and then the selection of the monomer type is determined by its compatibility with polymerization systems. In the determination step of the monomer structures, ease of synthetic route, solubility in the solvents, and reactivity with other reagents should be considered. However, in the determination step, the contribution of the molecular mobility of monomer structures to the interaction with target molecules is hardly considered. The design criteria of efficient multivalent polymer ligands should include the influence of molecular mobilities based on the monomer structures, when one considers that proteins adopt amide bonds for their backbone structures, and owing to the resultant suppressed rotational rigidity.[1] Furthermore, synthetic polymers that have flexible structures have been shown to exhibit a strong interaction with target molecules, which indicates that the molecular mobility of the biofunctional polymers is crucial for molecular recognition. [30–34]

In this work, the contribution of the monomer structures to the interaction with biomolecules is evaluated with respect to molecular mobility. The difference of molecular mobility derived from the representative monomer structures (acrylamide or acrylate) is quantitatively evaluated by differential scanning calorimetry (DSC) measurement and the T_2 relaxation time from proton nuclear magnetic resonance spectroscopy (^{1}H NMR). To prepare model polymers as multivalent ligands, a carbohydrate is adopted as a functional unit that recognizes the specific domains of target proteins (lectins).[35]

Glycopolymers bind to lectins through multivalent interactions between the multiple carbohydrate units in the side chains and carbohydrate-recognition domains (CRDs) on the surface of lectin. [36–39] The interaction of the glycopolymers is enhanced by an accumulation of the weak monovalent interactions of the carbohydrate and CRD. [40–43] The enhanced interaction of the glycopolymers is measured both by isothermal titration calorimetry (ITC) and by a hemagglutination inhibition assay (HI assay). The design criterion regarding the monomer structure is considered by the correlation between the molecular interaction and the molecular mobility.

Experimental Section

Materials.

Acryloyl chloride (98.0 %), 3-butyn-1-ol (97.0%), sodium azide (99.0 %), tetrakis(acetonitrile)copper(I) hexafluorophosphate ($[Cu(CH_3CN)_4]PF_6$, 97.0%), *N*, *N*-diisopropylethylamine (DIPEA, 99.0 %), sodium L-ascorbate ($_L$-Asc-Na, 98.0 %), 2-bromopropionic acid (98.0 %), and *n*-butanethiol (97.0%) were purchased from Tokyo Chemical Industry (TCI) Co., Ltd (Tokyo, Japan). Mannose, 3-butynyl amine (95.0%), sodium methoxide (95.0 %), triethylamine (TEA), carbon disulfide (98.0 %), 2,2'-azobis[2-(2-imidazolin-2-yl)propane]dihydrochloride (VA-044) (97.0 %), sodium nitrate (98.0 %), potassium chloride (99.5 %), and 4-dimethylaminopyridine (DMAP, 99.0 %) were purchased from FUJIFILM Wako Pure Chemical Corporation (Tokyo, Japan). The 2-Chloro-1,3-dimethylimidazolinium chloride (DMC) was purchased from Sigma-Aldrich (St. Lois, MO). Copper(II) sulfate (97.5 %), sodium hydrogen carbonate (99.0 %), and sodium chloride (99.0 %) were purchased from Kanto Chemical Co., Inc (Tokyo, Japan). Concanavalin A (ConA) and bovine serum albumin (BSA) were purchased from Funakoshi Co., Ltd (Tokyo, Japan). Mannose azide, 3-butynyl acrylamide, tris[(1-benzyl-1H-1,2,3-triazol-4-yl)methyl]amine (TBTA), and RAFT agent (SBTPA) were synthesized according to previous reports. [44–47]

Characterization.

Proton and carbon nuclear resonance (^{1}H and ^{13}C NMR) spectra were recorded on a JEOL-ECP400 spectrometer (JEOL, Tokyo, Japan) with $CDCl_3$ or D_2O as the solvent at room temperature. The spin-spin relaxation time (T_2) was measured at a concentration of 15 mg/mL in D_2O for all polymer samples. Size exclusion chromatography (SEC)

analysis was performed with a JASCO 980 high-performance liquid chromatography instrument with a Shodex OH pak SB-803 HQ column (Showa Denko, Tokyo, Japan), and peaks were detected with a JASCO RI-2031 Plus RI detector and a Viscotek triple detector array (Malvern Instruments Ltd., Worcestershire U.K.). SEC analyses were conducted at a flow rate of 0.5 mL/min by injecting 20 μL of a polymer solution (2 g/L) in an aqueous solution of 100 mM $NaNO_3$ as an eluent. Molecular weights were estimated using Pullulan standard (Shodex). All samples for SEC were treated with a 0.45 μm filter prior to the analysis. Dynamic light scattering (DLS) was performed on a ZETASIZER NANO-ZS90 (Malvern Instruments Ltd.) using a glass cuvette of a polymer solution (1 mg/mL) in PBS(+) buffer. All samples for DLS were filtered through a 0.45 μm filter prior to the analysis. DSC measurements were performed using a Hitachi High Tech Science X DSC7000. Scans were performed under a nitrogen atmosphere using a heating rate of 10 °C/min. ITC measurement was performed by a Microcal VP-ITC instrument.

Synthesis of 3-butynyl acrylate.

Triethylamine (4.05 mL, 29.2 mmol), 3-Butyn-1-ol (1.86 g, 2 mL, 26.5 mmol), and DMAP (162 mg, 1.33 mmol) were dissolved in dry dichloromethane (30 mL) and stirred in an ice bath. Acryloyl chloride (2.38 mL, 29.2 mmol) was slowly dropped into the solution and the mixture was stirred for 15 h at room temperature. The progress of the reaction was confirmed by thin layer chromatography (EtOAc : hexane = 1 : 1). The precipitate was filtered, and the filtrate was washed with 0.5 M HCl (aq) twice, saturated $NaHCO_3$ (aq) twice, and saturated brine once. The organic phase was dried with $MgSO_4$, filtered and concentrated under reduced pressure. The crude product was purified by silica

column chromatography (EtOAc : hexane = 1 : 1) to give 3-butynyl acrylate as a colorless oil (2.47 g, 75%). An inhibitor (4-methoxyphenol, 5 mg) was added, and the compound was kept in a fridge.

^{1}H NMR ($CDCl_3$, δ in ppm): 6.43 (dd, *J* = 1.6, 16.8 Hz, *trans* C**H**$_2$=CH, 1H), 6.13 (dd, *J* = 10.4, 16.8 Hz, CH_2=C**H**, 1H), 5.84 (dd, *J* = 1.6, 10.4 Hz, *cis* C**H**$_2$=CH, 1H), 4.26 (t, *J* = 6.8 Hz, -O-C**H**$_2$-CH_2-, 2H), 2.56 (ddd, *J* = 2.8, 6.8 Hz, -C**H**$_2$-C≡C, 2H), 2.00 (t, *J* = 2.8 Hz, C≡CH, 1H).

Synthesis of mannose acrylamide (MAm).

Mannose azide (1.52 g, 7.41 mmol), 3-Butynyl acrylamide (912 mg, 7.41 mmol), $[Cu(CH_3CN)_4]PF_6$ (276 mg, 0.74 mmol), and TBTA (393 mg, 0.74 mmol) were dissolved in a mixture of *t*-BuOH (100 mL) and H_2O (50 mL). The solution was stirred for 24 h at 30 °C under nitrogen atmosphere. The solution was concentrated under reduced pressure, and the precipitate was filtered. The crude product was purified by reverse-phase chromatography (gradient from water to methanol). The fraction containing the product was concentrated under reduced pressure and stirred with a metal scavenger (SiliaMets Imidazole) at room temperature overnight. After removal of the metal scavenger by filtration, the filtrate was concentrated under reduced pressure and the product was purified by reverse-phase chromatography again. The fraction was concentrated under reduced pressure and the mannose acrylamide (MAm) product was obtained as a white solid by freeze-drying (771 mg, 32 %).

^{1}H NMR (400 MHz, D_2O) δ in ppm: 7.89 (s, 1H, triazole), 6.11 (dd, 1H, *J* = 9.6 Hz, CH2=C**H**), 6.03 (dd, 1H, *J* = 1.6 Hz, C**H**2=CH), 5.99 (d, 1H, *J* = 2.4 Hz, anomer), 5.64 (dd, 1H, *J* = 1.6 Hz, C**H**2=CH),

4.70 (m, 1H, *J* = 1.2 Hz, Man), 4.01 (dd, 1H, *J* = 3.6 Hz, Man), 3.66-3.76 (m, 3H, Man), 3.49 (t, 2H, *J* = 6.8 Hz, NH-C**H**2-CH2), 3.16 (m, 1H, *J* = 3.2 Hz, Man), 2.90 (t, 2H, *J* = 6.8 Hz, CH2-C**H**2-triazole).

^{13}C NMR (400 MHz, D_2O) δ in ppm: 168.5 (-**C**ONH-, amide), 145.5 (CH2-**C**(N)=CH, triazole), 129.8 (CH2=**C**H), 127.2 (**C**H2=CH), 123.1 (C=**C**H-N, triazole), 86.6, 75.9, 70.4, 68.2, 66.5, 60.3 (Man), 38.7 (NH-**C**H2-CH2), 24.6 (CH2-**C**H2-C).

Synthesis of mannose acrylate (MAc).

Mannose azide (1.17 g, 5.70 mmol), 3-Butynyl acrylate (702 mg, 5.70 mmol), $[Cu(CH_3CN)_4]PF_6$ (213 mg, 0.57 mmol), and TBTA (303 mg, 0.57 mmol) were dissolved in a mixture of *t*-BuOH (80 mL) and H_2O (40 mL). The solution was stirred for 24 h at 30 °C under nitrogen atmosphere. Mannose acrylate (MAc) product was obtained as a white solid after purification in the same procedure as that for MAm (1.35 g, 72 %).

^{1}H NMR (400 MHz, D_2O) δ in ppm: 7.93 (s, 1H, triazole), 6.26 (dd, 1H, *J* = 0.8 Hz, CH2=CH), 6.04 (dd, 1H, *J* = 10.4 Hz, CH2=CH), 5.97 (d, 1H, *J* = 2.4 Hz, anomer), 5.84 (dd, 1H, *J* = 1.6 Hz, CH2=CH), 4.68 (m, 1H, Man), 4.37 (t, 2H, *J* = 6.4 Hz, O-CH2-CH2), 4.00 (dd, 1H, *J* = 3.6 Hz, Man), 3.64-3.74 (m, 3H, Man), 3.15 (m, 1H, *J* = 3.6 Hz, Man), 3.05 (t, 2H, *J* = 6.0 Hz, CH2-CH2-triazole).

^{13}C NMR (400 MHz, D_2O) δ in ppm: 168.3 (-COO-, ester), 144.7 (CH2-C(N)=CH, triazole), 132.3 (CH2=CH), 127.5 (CH2=CH), 123.4 (C=CH-N, triazole), 86.5, 76.0, 70.4, 68.3, 66.3, 63.5, 60.4 (O-CH2-CH2 and Man), 24.3 (CH2-CH2-C).

Synthesis of RAFT agent (SBTPA).

n-Butanethiol (5 mL, 4.2 g, 46.6 mmol) and triethylamine (13.0 mL, 9.49 g, 93.8 mmol) were added in $CHCl_3$ (30 mL) at 0 °C, and then stirred at room temperature for 30 min. Carbon disulfide (5.62 mL, 7.08 g, 93 mmol) was added at 0 °C then stirred at room temperature for 3 h. 2-Bromopropionic acid (4.16 mL, 7.11 g, 46.5 mmol) was added at room temperature, and stirred overnight. Cation exchange resin was added until the pH of the solution became 3–4, and the solution was stirred for 15 min. The resin was removed by filtration, and the solution was washed with Milli-Q water. The organic layer was concentrated under reduced pressure and purified by column chromatography using hexane/ethyl acetate as the eluent. The fraction containing the product was collected and concentrated under reduced pressure. The product was dissolved in MeOH, and saturated $NaHCO_3$(aq) was added at room temperature until the pH of the solution became 7–8. The solvent was removed under reduced pressure and by freeze drying. Excess amount of EtOH was added and the solid $NaHCO_3$ was filtered. The filtrate was removed under reduced pressure, and SBTPA was obtained as a yellow solid (4.94 g, 45%). ^{1}H NMR (400 MHz, D_2O) δ in ppm: 0.76 (t, 3H), 1.27 (sext, 2H), 1.39 (d, 3H), 1.54 (quin, 2H), 3.26 (t, 2H), 4.35 (q, 1H).

Polymerization procedure.

Polymerization was proceeded using RAFT polymerization. Glycomonomers, SBTPA, and initiator

(VA-044) were dissolved in Milli-Q water. Detailed information is provided in Table 1. The solution was degassed by freeze–thaw cycles (three times) and placed in an oil bath (70 °C) for 2 h. The reaction was stopped by exposure to air. Each gylcopolymer was purified by dialysis (MWCO: 3.5 kDa) against Milli-Q water overnight and was obtained as a solid after freeze drying.

Conformation analysis of the glycopolymers by molecular dynamics simulation.

Winmostar software with LAMMPS program was used for the simulation. To shorten the calculation time of the simulation, an annealing process was performed. The calculation conditions were set with reference to previous studies.[48] Two types of glycopolymers (acrylamide or acrylate) bearing mannose were prepared using the homopolymer building function. The stereoregularity was set as atactic, and the racemo ratio was 0.5. One polymer molecule and 27,000 water molecules were placed in an 8 × 13 × 8 nm^3 cell, and the set density was approximately 1.00 g/cm^3. In the NPT calculation, the temperature was 500 K and the "# of time steps" was 10,000. The energy change after the calculation was read and it was confirmed that various parameters had reached a steady state. Finally, the annealing process was performed while lowering the temperature. The final temperature was set at 300 K. After the annealing process was completed, the final structure was defined as the stable conformation of the glycopolymers in solution.

Differential scanning calorimetry (DSC) measurement.

Samples (1–2 mg) were prepared in a pan, and then hermetically sealed. Samples were conditioned at 30 °C followed by heating to 180 °C at a heating rate of 10 °C/min. The glass transition temperature (T_g) was reported as the inflection point of the heat flow thermograms taken from the third heating curve.

Isothermal titration calorimetry (ITC) measurement.

ConA and glycopolymers were dissolved in a solution of 10 mM acetate buffer (pH = 5.0) with $MgCl_2$ (1 mM), $CaCl_2$, (1 mM), and NaCl (30 mM). Solutions with concentration of ConA (15–30 μM) and glycopolymer (75–600 μM) were prepared. Titrations were performed at 25 °C with a stirring speed of 560 rpm. Injections of glycopolymer solution into the cell (cell volume: 1.413 mL) ranged from 3 to 5 μL at an interval of 276.65 s. The number of injections was set to 21 and the first injection was deleted before data analysis to obtain accurate data. The experimental data were fitted to a theoretical titration curve using Origin software supplied by Microcal. A standard One Set of Sites model was used with ΔH (enthalpy change in kcal/mol), K_a (binding constant in M^{-1}), and n (number of binding sites per monomer) as variable parameters.

Hemagglutination inhibition (HI) assay.

Phosphate-buffered saline solution with calcium and magnesium ions (PBS(+)) was added into a 96-

well plate (50 μL/well) except for the first lane. Con A in PBS(+) (1 mg/mL, 100 μL) was added into the first line of the 96-well plate, and the solution in the first lane was diluted by two steps (50 μL). Red blood cells (RBCs) in the purchased blood cell suspension were washed by centrifugation with PBS(-) three times. The concentrated RBCs were resuspended in PBS(+) (0.5 v/v%) and this was injected in each well (50 μL). The 96-well plate was incubated for 1 h at room temperature, and the lowest concentration of ConA required to aggregate the RBCs was determined. This process was triplicated, and the average value was defined as 1HAU.

PBS(+) solution was added into a 96-well plate (25 μL/well) except for the first lane. Glycopolymer solution in PBS(+) (2 mg/mL, 50 μL) was injected in the first lane. The solution in the first lane was diluted by two steps (25 μL). The ConA solution in PBS(+) (8 HAU) was injected in each well (25 μL/well). The 96-well plate was incubated for 1 h at room temperature. The RBCs resuspended in PBS(+) (0.5 v/v%) were injected in each well (50 μL). The 96-well plate was incubated for 2 h at room temperature (triplicated). Hemagglutination inhibition was observed.

Results and Discussion

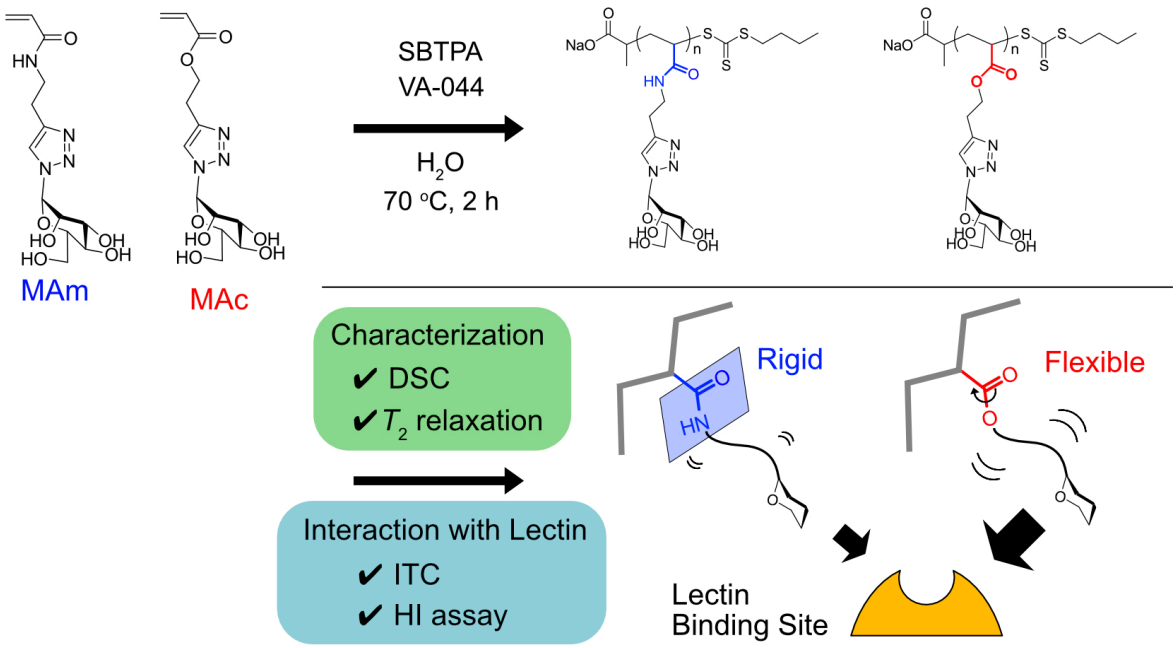

Preparation of glycopolymers by RAFT polymerization.

Glycopolymers bearing mannose units were synthesized by RAFT polymerization from two types of monomers: acrylamide and acrylate. Each glycomonomer containing mannose residue was synthesized by copper-catalyzed azide–alkyne cycloaddition of mannose azide and acrylic monomers with an alkyne moiety. The RAFT polymerization proceeded in aqueous solution in accordance with the previous reports.[26] To ensure the homogeneity of the monomer sequence among the synthesized polymers, homo-glycopolymers without any other co-monomers were prepared. The target degree of polymerization (D.P.) was set at 40, 80, 120, and 160. The monomer conversions were determined by ^{1}H NMR and were over 90 % for all polymerization conditions (Table 1). The relative molecular weight

(M_n) and polydispersity index (M_w/M_n) were characterized by SEC analysis. The relative molecular weights of the glycopolymers increased corresponding to the target D.P., and SEC traces of each glycopolymer sample showed a unimodal peak and relatively low polydispersity (Figure S2). The polydispersity of the acrylamide-type polymers (< 1.22) was narrower than that of the acrylate-type polymers (< 1.51), presumably owing to the high propagation rate of acrylamide monomers in water (Table 1).[49] These results indicated that well-controlled glycopolymers with different monomer structures were successfully synthesized by controlled radical polymerization.

Table 1. Properties of RAFT polymerization of polymer backbones.

Polymers	Backbone	Target D.P.	Feed ratio [M]: [CTA]: [I]	Conv.[a] (%)	D.P.[a] (mer)	$M_{n,th}$[b] (g/mol)	M_n[c] (g/mol)	M_w/M_n[c] (-)	D_h[d] (nm)
MAm_{40}	Acrylamide	40	40: 1: 0.04	>99	40	13,400	6,700	1.18	4.53
MAm_{80}		80	80: 1: 0.04	>99	79	26,200	11,200	1.20	5.69
MAm_{120}		120	120: 1: 0.04	>99	119	39,300	18,200	1.20	7.07
MAm_{160}		160	160: 1: 0.04	>99	160	52,800	23,100	1.22	7.77
MAc_{40}	Acrylate	40	40: 1: 0.02	>99	39	13,100	6,700	1.37	4.40
MAc_{80}		80	80: 1: 0.02	>99	80	26,600	11,000	1.43	5.93
MAc_{120}		120	120: 1: 0.02	>99	121	40,100	16,700	1.46	7.04
MAc_{160}		160	160: 1: 0.04	90	154	51,000	19,900	1.51	7.99

Monomer concentration of each polymerization ([M]) was set at 1.0 M. (a) Monomer conversion (Conv.) and the degree of polymerization (D.P.) were determined from ^{1}H NMR. (b) Theoretical molecular weight was calculated by following the formula: $M_{n,\,the} = MW_{CTA} + MW_{glycomonomer} \times$ D.P. (c) Relative molecular weight and polydispersity index were determined by size exclusion chromatography (SEC) analysis calibrated with a Pullulan standard. The eluent was 100 mM $NaNO_3$ (aq). (d) The hydrodynamic diameter (D_h) was estimated by dynamic light scattering (DLS) measurement in PBS (-) buffer (1g/L).

The hydrodynamic diameters (D_hs) of the glycopolymers were determined by DLS measurement, and the value increased with the target D.P. of the glycopolymers (Figure S3). It is noteworthy that the D_h values of the acrylamide-type and acrylate-type glycopolymers with the same D.P. almost corresponded to each other and were not dependent on the difference of the monomer structures (amide or ester bond in the side chains). To support the results of DLS measurement, the conformations of the synthesized glycopolymers were simulated by molecular dynamics simulation. Images of the two types of glycopolymers after the annealing process are shown in Figure S4 (the surrounding water molecules are hidden). Both types of glycopolymers had a similar conformation in water (random-coil conformation), and no definite self-folding was observed.

Characterization of physical properties of glycopolymers by DSC measurement.

To reveal the difference of molecular mobilities of the glycopolymers, the synthesized polymers were characterized by DSC measurement. The samples were heated from room temperature, and the T_g was determined. The T_g values of the acrylamide-type and acrylate-type glycopolymers were approximately 160 °C and 118 °C, respectively (Table 2). For both types of glycopolymers, the T_g values were totally different and dependent not on the polymer length (the degree of polymerization) but on the monomer structures. The T_g of the acrylamide-type glycopolymers was higher than that of the acrylate-type polymers, which arose from the rigidity of the amide bonds in the side chains.

Table 2. T_g and T_2 of the glycopolymers at each peak of the chemical shifts[a].

	T_g (°C)	$T_2^{1.5\ ppm}$ (ms)	$T_2^{6.0\ ppm}$ (ms)
MAm_{40}	158.1	12.9 ± 1.4	168.9 ± 2.5
MAm_{80}	160.7	8.7 ± 0.2	118.7 ± 2.9
MAm_{120}	159.9	7.8 ± 0.2	109.3 ± 0.6
MAm_{160}	162.2	6.3 ± 0.1	100.4 ± 4.8
MAc_{40}	117.0	12.6 ± 0.4	223.4 ± 2.6
Mac_{80}	118.3	9.9 ± 0.3	194.0 ± 1.4
MAc_{120}	117.6	9.1 ± 0.0	166.7 ± 1.5
MAc_{160}	117.2	7.5 ± 0.1	169.4 ± 2.5
[a]Solvent was D_2O (15 mg/mL).			

Mobility analysis of glycopolymers by spin-spin relaxation (T_2) time measurement using ^1H NMR.

According to the difference in the T_g, it was anticipated that the synthesized glycopolymers would have different molecular mobilities based on the monomer types. Generally, the interactions of the glycopolymers with target biomolecules are evaluated in a solution, and thus, the molecular mobility of the glycopolymers should be evaluated in a solution. The molecular mobilities both of the polymer backbones and the side chains of the glycopolymers in water were characterized by the spin-spin (T_2) relaxation time analysis using ^{1}H NMR. In the case of macromolecules, the T_2 relaxation time is influenced both by the overall rotatory diffusion of polymer molecules and by the local segment motion.[50–54] However, local segment motion is much faster than overall rotatory diffusion and contributes to the T_2 relaxation time more than the latter. Longer T_2 relaxation indicates a higher rotational mobility of the polymer molecules. The two peaks shown in ^{1}H NMR spectra were selected

to determine the molecular mobility. The first peak was derived from the protons of the main chain (1.4–1.5 ppm), and the second peak was derived from the anomeric proton of mannose in the side chain (5.8–6.0 ppm). The T_2 relaxation time of the side chain was longer than that of the polymer backbones, which suggested that the molecular mobility of the side chains was higher than the polymer backbones (Table 2 and Figure 2). Compared with acrylamide glycopolymers, acrylate glycopolymers showed a longer T_2 relaxation time, and the molecular mobility of the acrylate-type glycopolymers seemed to be higher than that of the acrylamide-type polymers. This arose from the difference of free rotation between amide and ester bonds. The amide bond of acrylamide has a resonance structure, and the free rotation of the C-N bond is restricted. In contrast, free rotation of the ester bond of acrylate is not especially restricted.[1,55] This difference of rotational mobility influences the molecular mobility of the mannose units in the side chains.

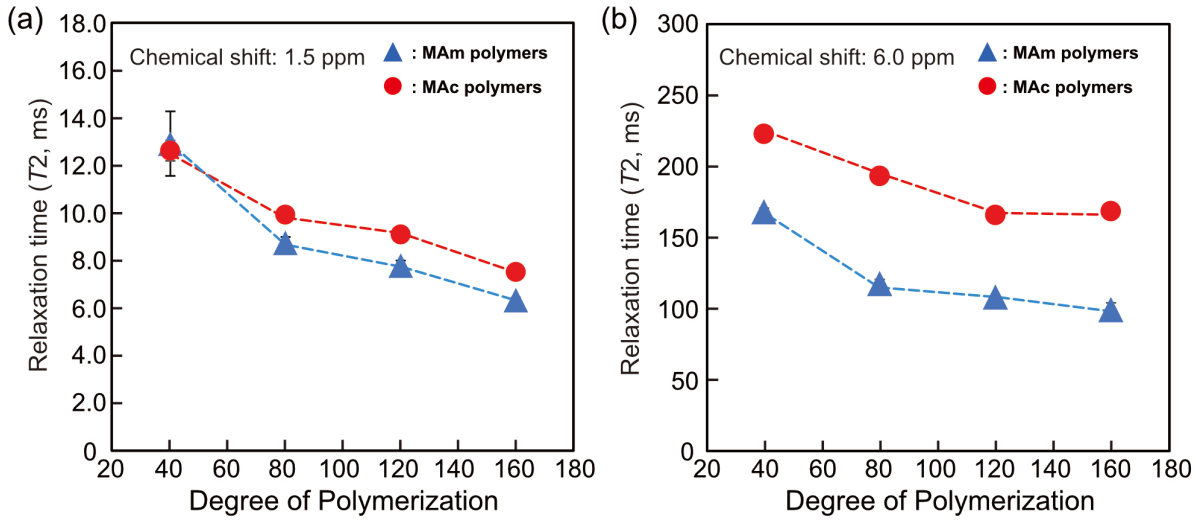

Figure 2. Plots of the T_2 for the glycopolymers at each peak of the chemical shifts: (a) 1.5 ppm and (b) 6.0 ppm in D_2O. The blue triangles and red circles represent the MAm and MAc polymer series, respectively.

Evaluation of the interaction of the glycopolymers with ConA by isothermal titration calorimetry.

The interaction between glycopolymers and a model lectin, ConA was quantitatively evaluated by ITC measurement. ConA is a *C*-type lectin composed of four subunits.[35] One subunit has one CRD (in total four CRDs per one ConA molecule), and each CRD selectively binds to a mannose unit. A preliminary ITC experiment using neutral PBS(+) buffer solution revealed the appearance of an aggregation of ConA, as has been reported in previous studies.[56] Thus, in accordance with the previous report, an acidic buffer was used for ITC measurements to avoid aggregation of ConA. ConA forms a dimer at acidic pH, but forms a tetramer at neutral pH.[57] Therefore, in this work, all experiments were carried out in 10 mM acetate buffer (pH = 5.0) for ITC measurement.[58]

ITC titration curves of the ConA solution demonstrated an exotherm with sequential injections of the glycopolymers (MAm_{120} or MAc_{120}) whereas those of the BSA solution did not (Figure S5 and S6). This indicated that the synthesized glycopolymers exhibited molecular recognition based on the carbohydrate–lectin interaction. The results of ITC measurement of glycopolymers are shown in Table 3. The binding constant (K_a: M^{-1}), enthalpy change (ΔH: kcal/mol), entropy change ($-T\Delta S$: kcal/mol), and binding stoichiometry (n) were evaluated by fitting the raw titration curve data using the One Set of Sites model.[59] To confirm the accuracy of the measurement, the c values ($c = n*[\text{ConA}]*K_a$), which are an index of accurate experimental values, were calculated.[60] Wisemann *et. al.* suggested that reliable experiment affords a range of c values from 1 to 1000.[61] The results in Table 3 gave a range from 1 to 16, which demonstrated an accuracy. The K_a values of MAm_{40} to MAm_{160} and MAc_{40} to

MAc_{160} were 0.19, 0.77, 2.05, 3.12 ($\times 10^6$ M^{-1}), and 0.47, 2.70, 4.20, 8.03 ($\times 10^6$ M^{-1}), respectively (Figure 3). The K_a values increased as the D.P. of the glycopolymers increased, which arose from the multivalent binding to ConA. Interestingly, while the two types of glycopolymers had the same polymer structures except for the monomer types (amide or ester bond in the side chains), the binding constants of the acrylate glycopolymers were approximately 2 or 3 times higher than those of the acrylamide type for each polymer length. Considering that the two types of glycopolymers had similar D_h values (Table 1), the difference of the interaction depended not on the polymer conformation in the solvent but on the molecular mobility.

Table 3. Thermodynamic parameters for the binding of glycopolymers to Con A.

Polymers	Backbone	K_a (10^6 M^{-1})	ΔH (kcal/mol)	$-T\Delta S$ (kcal/mol)	n^a (-)	c (-)
MAm_{40}	Acrylamide	0.19 ± 0.010	−26.8 ± 1.9	19.6 ± 1.9	0.34	1.3
MAm_{80}		0.77 ± 0.070	−36.2 ± 0.40	28.2 ± 0.42	0.20	2.8
MAm_{120}		2.05 ± 0.18	−50.3 ± 0.63	41.7 ± 0.64	0.15	4.7
MAm_{160}		3.12 ± 0.80	−57.7 ± 3.0	48.9 ± 3.1	0.13	6.1
MAc_{40}	Acrylate	0.47 ± 0.040	−26.1 ± 0.57	18.3 ± 0.63	0.31	2.7
MAc_{80}		2.70 ± 0.54	−39.5 ± 0.49	30.8 ± 0.61	0.21	10.7
MAc_{120}		4.20 ± 0.22	−53.6 ± 1.5	44.2 ± 1.5	0.17	10.5
MAc_{160}		8.03 ± 0.50	−68.9 ± 1.1	59.3 ± 1.1	0.12	15.0
(a) The binding stoichiometry was determined by the inflection point.						

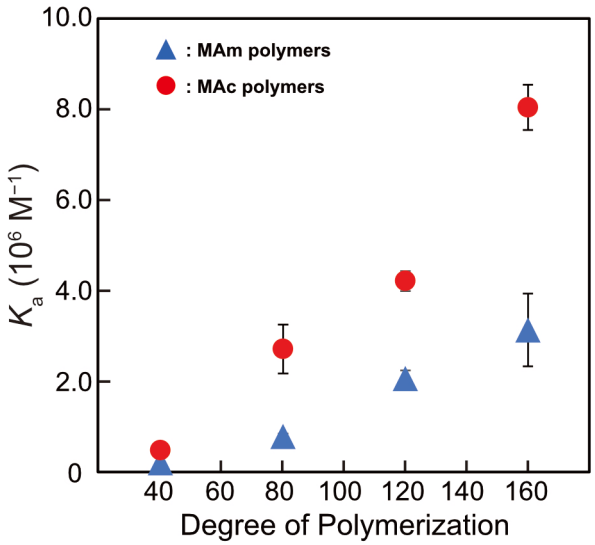

Figure 3. Plots of the K_a of the glycopolymers for dimeric ConA: (a), (b) ΔH, and (c) $-T\Delta S$. The blue triangles and red circles represent the MAm and MAc polymer series, respectively.

The carbohydrate–lectin interaction is largely contributed by hydrogen bonds and is driven by the enthalpy change. The enthalpy change ΔH of MAm_{40} to MAm_{160} and MAc_{40} to MAc_{160} were −26.8, −36.2, −50.3, −57.7 (kcal/mol), and −26.1, −39.5, −53.6, −68.9 (kcal/mol), respectively (Figure S7a). A decrease of ΔH to the negative side was observed as the D.P. increased, which indicated that the longer polymer length was favorable for the interaction with ConA. The multiple binding of the glycopolymers to ConA caused this change of ΔH. Furthermore, the acrylate glycopolymers showed lower values than the acrylamide glycopolymers, so the structure of acrylate monomers was more favorable for the interaction than the acrylamide monomers. Similarly, $-T\Delta S$ of MAm_{40} to MAm_{160} and MAc_{40} to MAc_{160} were 19.6, 28.2, 41.7, 48.9 (kcal/mol), and 18.3, 30.8, 44.2, 59.3 (kcal/mol), respectively (Figure S7b). For both types of glycopolymers, the increase of $-T\Delta S$ to the positive side

was observed as the D.P. increased. As expected from the T_2 measurement, the acrylate glycopolymers showed higher values of $-T\Delta S$ than the acrylamide glycopolymers, which was unfavorable for the interaction. This indicated that the molecular mobility of the acrylate glycopolymers was more restricted in binding to ConA than that of the acrylamide glycopolymers. The values of ΔH and $-T\Delta S$ showed the trends of enthalpy-entropy compensation, which is also observed in other interactions of biomolecules (Figure S8).[62]

Thermodynamic parameters were dependent on the monomer structures, and the acrylate-type glycopolymers showed a favorable ΔH and an unfavorable $-T\Delta S$ change more than those of the acrylamide-type. These differences of binding parameters resulted from the difference of the molecular mobility based on the monomer structures. Mannose units tethered to the polymer backbone through an ester bond have a higher molecular mobility than those with an amide bond, and the increased probability of binding to the CRDs of ConA leads to a higher enthalpy gain. However, the molecular mobility of mannose units with an ester bond decreases for binding to ConA more than that of those with an amide bond, which invokes a large entropy loss. These slight differences in thermodynamic parameters demonstrate that different monomer structures affect the interaction of the glycopolymers with ConA, and the structure with rotational freedom exhibit the higher binding constant.

Interaction of the synthesized glycopolymers with ConA by the HI assay.

The interaction of the glycopolymers with tetrameric ConA was also evaluated by the HI assay.

The pH of the solution was neutral, where ConA has the tetrameric structure. The synthesized glycopolymers except MAm_{40} inhibited RBC aggregation in the treated concentration range (Figures 4 and S9). The minimum polymer concentration for hemagglutination inhibition was defined as an inhibition constant, K_i, and the strength of the interaction of each glycopolymer with ConA was evaluated.[8,41] The K_i values were calculated by the mannose unit concentration, with a lower K_i indicating a stronger interaction with ConA. The K_i values of MAm_{80}, MAm_{120}, and MAm_{160} were determined to be 5.1×10^{-4}, 2.0×10^{-3}, and 2.0×10^{-3} mol/L, respectively. Similar to the results of the ITC measurement, the K_i values of acrylate-type glycopolymers were lower than those of acrylamide-type glycopolymers ($K_i = 1.0 \times 10^{-3}$, 9.5×10^{-5}, 4.7×10^{-5} and 6.3×10^{-5} mol/L for MAc_{40}, MAc_{80}, MAc_{120}, and MAc_{160}, respectively). For both types of the glycopolymers, the K_i values of the glycopolymers with a longer polymer length were dramatically higher than those of the short polymers. This arose from the change of the binding mode from one-site binding to two-site binding, and the thresholds of the polymer length were between 40 and 80 for both types of the glycopolymers.[23,26] The difference of the strength of the interactions for the monomer type was observed not only in the ITC measurement but also in the HI assay, which suggested that the monomer type affected the intermolecular interaction through the molecular mobility of the mannose units in the side chains.

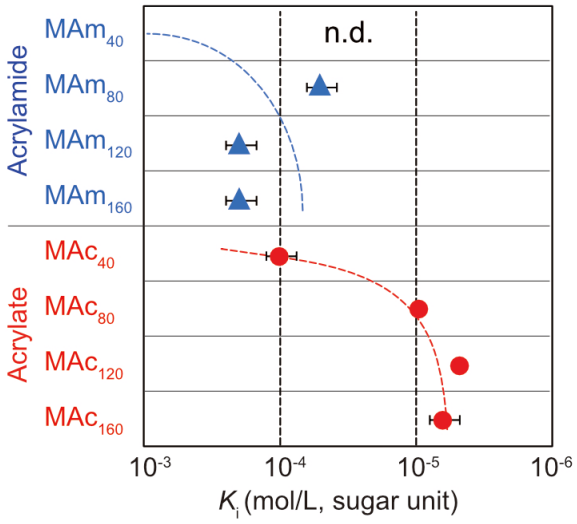

Figure 4. Plots of K_i from HI assay of the glycopolymers against ConA (triplicated). The unit is sugar concentration. The error bars indicate ± σ. The dash lines were drawn for guiding purpose.

Conclusions

We focused on the monomer structures of biofunctional polymers, acrylamide and acrylate, and the effect of the monomer types on molecular recognition was evaluated. Physical properties of the synthesized glycopolymers were characterized by DSC and ^{1}H NMR spin-spin relaxation time measurements. The monomer structures affected T_g and T_2 of the glycopolymers, and the acrylate-type glycopolymers showed a higher molecular mobility. The interactions of the synthesized glycopolymers were quantitatively evaluated by ITC measurement, and the thermodynamic parameters of the glycopolymers were determined. The acrylate-type glycopolymers exhibited the higher binding constant, greater enthalpy gain, and larger entropy loss. In the HI assay, the two types of glycopolymers exhibited showed different HI inhibition against ConA, and the acrylate-type glycopolymers showed a stronger interaction than the acrylamide-type glycopolymers even though there was only a slight difference in the monomer structures. This agreed with the results of the ITC measurement and, furthermore, the difference could not be explained by the multivalence effects alone. Therefore, the slight difference of the monomer structures affected the molecular mobility of the mannose units in the side chains, which led to the different interactions of the glycopolymers with ConA. The acrylate-type glycopolymers had a rotational freedom of the side chains and exhibited a stronger interaction with the target lectin. This is one example of an interaction between biofunctional polymers and target molecules; however, the influence of the monomer structures on the interactions of the synthetic biofunctional polymers is not negligible. This study suggests that the design of the polymer backbone

is important in designing synthetic biofunctional polymers. There are various types of biopolymers such as proteins, nucleic acids, and polysaccharides, which have different physicochemical properties and roles. We believe that our study represents the importance of the physical properties of polymers to the molecule, which is important for elucidating the role of biopolymers.

Supporting Information

^{1}H NMR spectra of the obtained compounds (Figure S1), SEC chromatographs of the synthesized glycopolymers (Figure S2), DLS distributions of the glycopolymers (Figure S3), images of the simulated conformation of the glycopolymers (Figure S4), titration curves of ITC measurement (Figures S5 and S6), plots of the binding parameters from ITC measurement (Figure S7), enthalpy-entropy compensation plot obtained from ITC results (Figure S8), and results of the HI assay (Figure S9) are shown in the Supporting Information.

Acknowledgments

We acknowledge financial support from a Grant-in- Aid for Scientific Research (B) (JP19H0276) and a Grant-in-Aid for Scientific Research on Innovative Areas (JP20H05230 and JP20H04825).

Reference:

(1) Avan, I.; Hall, C. D.; Kartritzky, A. R. Peptidomimetics via modifications of amino acids and peptide bonds. *Chem. Soc. Rev.* **2014**, *43* (10), 3575–3594.

(2) Eildal, J. N. N.; Hultqvist, G.; Balle, T.; Stuhr-Hansen, N.; Padrah, S.; Gianni, S.; Strømgaard, K.; Jemth, P. Probing the Role of Backbone Hydrogen Bonds in Protein−Peptide Interactions by Amide-to-Ester Mutations. *J. Am. Chem. Soc.* **2013**, *135* (35), 12998–13007.

(3) Kosugi, T.; Hayashi, S. Crucial Role of Protein Flexibility in Formation of a Stable Reaction Transition State in an α-Amylase Catalysis. *J. Am. Chem. Soc.* **2012**, *134* (16), 7045–7055.

(4) Daniel, R. M.; Dunn, R. V.; Finney, J. L.; Smith, J. C. The Role of Dynamics in Enzyme Activity. *Annu. Rev. Biophys. Biomol. Struct.* **2003**, *32*, 69–92.

(5) García-Meseguer, R.; Martí, S.; Ruiz-Pernía, J. J.; Moliner, V.; Tuñón, I. Studying the Role of Protein Dynamics in an S_N2 Enzyme Reaction Using Free-Energy Surfaces and Solvent Coordinates. *Nat. Chem.* **2013**, *5* (7), 566–571.

(6) Wei, G.; Xi, W.; Nussinov, R.; Ma, B. Protein Ensembles: How Does Nature Harness Thermodynamic Fluctuations for Life? The Diverse Functional Roles of Conformational Ensembles in the Cell. *Chem. Rev.* **2016**, *116* (11), 6516–6551.

(7) Hanoian, P.; Liu, C. T.; Hammes-Schiffer, S.; Benkovic, S. Perspectives on Electrostatics and Conformational Motions in Enzyme Catalysis. *Acc. Chem. Res.* **2015**, *48* (2), 482–489.

(8) Mammen, M.; Choi, S. K.; Whitesides, G. M. Polyvalent Interactions in Biological Systems:

Implications for Design and Use of Multivalent Ligands and Inhibitors. *Angew. Chem Int. Ed.* **1998**, *37* (20), 2754–2794.

(9) Di Iorio, D.; Verheijden, M. L.; Van Der Vries, E.; Jonkheijm, P.; Huskens, J. Weak Multivalent Binding of Influenza Hemagglutinin Nanoparticles at a Sialoglycan-Functionalized Supported Lipid Bilayer. *ACS Nano* **2019**, *13* (3), 3413–3423.

(10) Liese, S.; Netz, R. R. Quantitative Prediction of Multivalent Ligand-Receptor Binding Affinities for Influenza, Cholera, and Anthrax Inhibition. *ACS Nano* **2018**, *12* (5), 4140–4147.

(11) Kitov, P. I.; Bundle, D. R. On the Nature of the Multivalency Effect: A Thermodynamic Model. *J. Am. Chem. Soc.* **2003**, *125* (52), 16271–16284.

(12) Tjandra, K. C.; Thordarson, P. Multivalency in Drug Delivery–When Is It Too Much of a Good Thing? *Bioconjugate Chem.* **2019**, *30* (3), 503–514.

(13) Fasting, C.; Schalley, C. A.; Weber, M.; Seitz, O.; Hecht, S.; Koksch, B.; Dernedde, J.; Graf, C.; Knapp, E. W.; Haag, R. Multivalency as a Chemical Organization and Action Principle. *Angew. Chem. Int. Ed.* **2012**, *51* (42), 10472–10498.

(14) Fox, J. M.; Zhao, M.; Fink, M. J.; Kang, K.; Whitesides, G. M. The Molecular Origin of Enthalpy/Entropy Compensation in Biomolecular Recognition. *Annu. Rev. Biophys.* **2018**, *47*, 223–250.

(15) Diehl, C.; Engstrom, O.; Delaine, T.; Håkansson, M.; Genheden, S.; Modig, K.; Leffler, H.; Ryde, U.; Nilsson, U. J.; Akke, M. Protein Flexibility and Conformational Entropy in Ligand Design

Targeting the Carbohydrate Recognition Domain of Galectin-3. *J. Am. Chem. Soc.* **2010**, *132* (41), 14577–14589.

(16) Tzeng, S. R.; Kalodimos, C. G. Protein activity regulation by conformational entropy. *Nature* **2012,** *488*, 236–240.

(17) Lutz, J. F.; Lehn, J. M.; Meijer, E. W.; Matyjaszewski, K. From Precision Polymers to Complex Materials and Systems. *Nat. Rev. Mater.* **2016**, *1*, 16024.

(18) Van Genabeek, B.; Lamers, B. A. G.; Hawker, C. J.; Meijer, E. W.; Gutekunst, W. R.; Schmidt, B. V. K. J. Properties and Applications of Precision Oligomer Materials; Where Organic and Polymer Chemistry Join Forces. *J. Polym. Sci.* **2021**, *59* (5), 373–403.

(19) Yang, C.; Flynn, J. P.; Niu, J. Facile Synthesis of Sequence-Regulated Synthetic Polymers Using Orthogonal SuFEx and CuAAC Click Reactions. *Angew. Chem. Int. Ed.* **2018**, *57* (49), 16194–16199.

(20) Ladmiral, V.; Mantovani, G.; Clarkson, G. J.; Cauet, S.; Irwin, J. L.; Haddleton, D. M. Synthesis of Neoglycopolymers by a Combination of "Click Chemistry" and Living Radical Polymerization. *J. Am. Chem. Soc.* **2006**, *128* (14), 4823–4830.

(21) Moraes, J.; Peltier, R.; Gody, G.; Blum, M.; Recalcati, S.; Klok, H. A.; Perrier, S. Influence of Block versus Random Monomer Distribution on the Cellular Uptake of Hydrophilic Copolymers. *ACS Macro Lett.* **2016**, *5* (12), 1416–1420.

(22) Lavilla, C.; Yilmaz, G.; Uzunova, V.; Napier, R.; Becer, C. R.; Heise, A. Block-Sequence-Specific

Glycopolypeptides with Selective Lectin Binding Properties. *Biomacromolecules* **2017**, *18* (6), 1928–1936.

(23) Jono, K.; Nagao, M.; Oh, T.; Sonoda, S.; Hoshino, Y.; Miura, Y. Controlling the Lectin Recognition of Glycopolymers via Distance Arrangement of Sugar Blocks. *Chem. Commun.* **2017**, *54* (1), 82–85.

(24) Grubbs, R. B.; Grubbs, R. H. 50th Anniversary Perspective: Living Polymerization - Emphasizing the Molecule in Macromolecules. *Macromolecules* **2017**, *50* (18), 6979–6997.

(25) Gody, G.; Maschmeyer, T.; Zetterlund, P. B.; Perrier, S. Rapid and Quantitative One-Pot Synthesis of Sequence-Controlled Polymers by Radical Polymerization. *Nat. Commun.* **2013**, *4*, 2505.

(26) Nagao, M.; Hoshino, Y.; Miura, Y. Quantitative Preparation of Multiblock Glycopolymers Bearing Glycounits at the Terminal Segments by Aqueous Reversible Addition–Fragmentation Chain Transfer Polymerization of Acrylamide Monomers. *J. Polym. Sci. Part A Polym. Chem.* **2019**, *57* (8), 857–861.

(27) Perrier, S. 50th Anniversary Perspective: RAFT Polymerization - A User Guide. *Macromolecules* **2017**, *50* (19), 7433–7447.

(28) Anastasaki, A.; Nikolaou, V.; Haddleton, D. M. Cu(0)-Mediated Living Radical Polymerization: Recent Highlights and Applications; A Perspective. *Polym. Chem.* **2016**, *7* (5), 1002–1026.

(29) Zhang, Q.; Wilson, P.; Li, Z.; McHale, R.; Godfrey, J.; Anastasaki, A.; Waldron, C.; Haddleton, D. M. Aqueous Copper-Mediated Living Polymerization: Exploiting Rapid Disproportionation of

CuBr with Me_6TREN. *J. Am. Chem. Soc.* **2013**, *135* (19), 7355–7363.

(30) Hoshino, Y.; Nakamoto, M.; Miura, Y. Control of Protein-Binding Kinetics on Synthetic Polymer Nanoparticles by Tuning Flexibility and Inducing Conformation Changes of Polymer Chains. *J. Am. Chem. Soc.* **2012**, *134* (37), 15209–15212.

(31) Nakamoto, M.; Hoshino, Y.; Miura, Y. Effect of Physical Properties of Nanogel Particles on the Kinetic Constants of Multipoint Protein Recognition Process. *Biomacromolecules* **2014**, *15* (2), 541–547.

(32) Ooya, T.; Utsunomiya, H.; Eguchi, M.; Yui, N. Rapid Binding of Concanavalin A and Maltose-Polyrotaxane Conjugates Due to Mobile Motion of α-Cyclodextrins Threaded onto a Poly(Ethylene Glycol). *Bioconjug. Chem.* **2005**, *16* (1), 62–69.

(33) Ooya, T.; Eguchi, M.; Yui, N. Supramolecular Design for Multivalent Interaction: Maltose Mobility along Polyrotaxane Enhanced Binding with Concanavalin A. *J. Am. Chem. Soc.* **2003**, *125* (43), 13016–13017.

(34) Nagao, M.; Matsubara, T.; Hoshino, Y.; Sato, T.; Miura, Y. Synthesis of Various Glycopolymers Bearing Sialyllactose and the Effect of Their Molecular Mobility on Interaction with the Influenza Virus. *Biomacromolecules* **2019**, *20* (7), 2763–2769.

(35) Ambrosi, M.; Cameron, N. R.; Davis, B. G. Lectins: Tools for the Molecular Understanding of the Glycocode. *Org. Biomol. Chem.* **2005**, *3* (9), 1593–1608.

(36) Miura, Y.; Hoshino, Y.; Seto, H. Glycopolymer Nanobiotechnology. *Chem. Rev.* **2016**, *116* (4),

1673–1692.

(37) Kiessling, L. L.; Grim, J. C. Glycopolymer Probes of Signal Transduction. *Chem. Soc. Rev.* **2013**, *42* (10), 4476–4491.

(38) Yilmaz, G.; Becer, C. R. Precision Glycopolymers and Their Interactions with Lectins. *Eur. Polym. J.* **2013**, *49* (10), 3046–3051.

(39) Ting, S. R. S.; Chen, G.; Stenzel, M. H. Synthesis of Glycopolymers and Their Multivalent Recognitions with Lectins. *Polym. Chem.* **2010**, *1* (9), 1392–1412.

(40) Loka, R. S.; McConnell, M. S.; Nguyen, H. M. Studies of Highly-Ordered Heterodiantennary Mannose/Glucose-Functionalized Polymers and Concanavalin A Protein Interactions Using Isothermal Titration Calorimetry. *Biomacromolecules* **2015**, *16* (12), 4013–4021.

(41) Nagao, M.; Fujiwara, Y.; Matsubara, T.; Hoshino, Y.; Sato, T.; Miura, Y. Design of Glycopolymers Carrying Sialyl Oligosaccharides for Controlling the Interaction with the Influenza Virus. *Biomacromolecules* **2017**, *18* (12), 4385–4392.

(42) Chen, Y.; Lord, M. S.; Piloni, A.; Stenzel, M. H. Correlation between Molecular Weight and Branch Structure of Glycopolymers Stars and Their Binding to Lectins. *Macromolecules* **2015**, *48* (2), 346–357.

(43) Lu, J.; Fu, C.; Wang, S.; Tao, L.; Yan, L.; Haddleton, D. M.; Chen, G.; Wei, Y. From Polymer Sequence Control to Protein Recognition: Synthesis, Self-Assembly and Lectin Binding. *Macromolecules* **2014**, *47* (14), 4676–4683.

(44) Ferguson, C. J.; Hughes, R. J.; Nguyen, D.; Pham, B. T. T.; Gilbert, R. G.; Serelis, A. K.; Such, C. H.; Hawkett, B. S. Ab Initio Emulsion Polymerization by RAFT-Controlled Self-Assembly. *Macromolecules* **2005**, *38* (6), 2191–2204.

(45) Brassard, C. J.; Zhang, X.; Brewer, C. R.; Liu, P.; Clark, R. J.; Zhu, L. Cu(II)-Catalyzed Oxidative Formation of 5,5′-Bistriazoles. *J. Org. Chem.* **2016**, *81* (24), 12091–12105.

(46) Tanaka, T.; Nagai, H.; Noguchi, M.; Kobayashi, A.; Shoda, S. I. One-Step Conversion of Unprotected Sugars to β-Glycosyl Azides Using 2-Chloroimidazolinium Salt in Aqueous Solution. *Chem. Commun.* **2009**, 3378–3379.

(47) Nagao, M.; Kurebayashi, Y.; Seto, H.; Takahashi, T.; Suzuki, T.; Hoshino, Y.; Miura, Y. Polyacrylamide Backbones for Polyvalent Bioconjugates Using “Post-Click” Chemistry. *Polym. Chem.* **2016**, *7* (38), 5920–5924.

(48) Meng, Y.; Shi, X.; Cai, L.; Zhang, S.; Ding, K.; Nie, S.; Luo, C.; Xu, X.; Zhang, L. Triple-Helix Conformation of a Polysaccharide Determined with Light Scattering, AFM, and Molecular Dynamics Simulation. *Macromolecules* **2018**, *51* (24), 10150–10159.

(49) Valdebenito, A.; Encinas, M. V. Effect of Solvent on the Free Radical Polymerization of *N*,*N*-Dimethylacrylamide. *Polym. Int.* **2010**, *59* (9), 1246–1251.

(50) Igumenova, T. I.; Frederick, K. K.; Wand, A. J. Characterization of the Fast Dynamics of Protein Amino Acid Side Chains Using NMR Relaxation in Solution. *Chem. Rev.* **2006**, *106* (5), 1672–1699.

(51) Jarymowycz, V. A.; Stone, M. J. Fast Time Scale Dynamics of Protein Backbones: NMR Relaxation Methods, Applications, and Functional Consequences. *Chem. Rev.* **2006**, *106* (5), 1624–1671.

(52) Heatley, F. Nuclear Magnetic Relaxation of Synthetic Polymers in Dilute Solution. *Prog. Nucl. Magn. Res. Spec.* **1979**, *13* (1), 47–85.

(53) Mccall, D. W. Nuclear Magnetic Resonance Studies of Molecular Relaxation Mechanisms in Polymers. *Acc. Chem. Res.* **1971**, *4* (6), 223–232.

(54) Chávez, F. V.; Saalwächter, K. Time-Domain NMR Observation of Entangled Polymer Dynamics: Universal Behavior of Flexible Homopolymers and Applicability of the Tube Model. *Macromolecules* **2011**, *44* (6), 1549–1559.

(55) Liebman, J. F.; Greenberg, A. The Origin of Rotational Barriers in Amides and Esters. *Biophys. Chem.* **1974**, *1*, 222–226.

(56) Xie, Y.; Peng, C.; Gao, Y.; Liu, X.; Liu, T.; Joy, A. Mannose-Based Graft Polyesters with Tunable Binding Affinity to Concanavalin A. *J. Polym. Sci. Part A Polym. Chem.* **2017**, *55* (23), 3908–3917.

(57) Silvers, T. R.; Myers, J. K. Osmolyte Effects on the Self-Association of Concanavalin a: Testing Theoretical Models. *Biochemistry* **2013**, *52* (51), 9367–9374.

(58) Boden, S.; Reise, F.; Kania, J.; Lindhorst, T. K.; Hartmann, L. Sequence-Defined Introduction of Hydrophobic Motifs and Effects in Lectin Binding of Precision Glycomacromolecules. *Macromol. Biosci.* **2019**, *19*, 1800425.

(59) Liu, Z.; Zhu, Y.; Ye, W.; Wu, T.; Miao, D.; Deng, W.; Liu, M. Synthesis of Well-Defined Glycopolymers with Highly Ordered Sugar Units in the Side Chain: via Combining CuAAC Reaction and ROMP: Lectin Interaction Study in Homo- and Hetero-Glycopolymers. *Polym. Chem.* **2019**, *10* (29), 4006–4016.

(60) Turnbull, W. B.; Daranas, A. H. On the Value of c: Can Low Affinity Systems Be Studied by Isothermal Titration Calorimetry? *J. Am. Chem. Soc.* **2003**, *125* (48), 14859–14866.

(61) Wiseman, T.; Williston, S.; Brandts, J. F.; Lin, L. N. Rapid Measurement of Binding Constants and Heats of Binding Using a New Titration Calorimeter. *Anal. Biochem.* **1989**, *179* (1), 131–137.

(62) Olsson, T. S. G.; Ladbury, J. E.; Pitt, W. R.; Williams, M. A. Extent of enthalpy–entropy compensation in protein–ligand interactions. *Protein Sci.* **2011**, *20*, 1607–1618.

Table of Contents graphic.

For Table of Contents Use Only.

Title: Influence of Monomer Structures for Polymeric Multivalent Ligands: Consideration of the Molecular Mobility of Glycopolymers

Authors: Masanori Nagao*, Masaya Kichize, Yu Hoshino, and Yoshiko Miura*